Published in final edited form as:
Neuron. 2010 March 25; 65(6): 859–872. doi:10.1016/j.neuron.2010.03.009.

NMDA receptors activated by subventricular zone astrocytic glutamate are critical for neuroblast survival prior to entering a synaptic network

Jean-Claude Platel[1], **Kathleen A. Dave**[1], **Valerie Gordon**[1], **Benjamin Lacar**[1], **Maria E. Rubio**[2], and **Angélique Bordey**[1]

[1] Departments of Neurosurgery, and Cellular and Molecular Physiology, Yale University School of Medicine, New Haven, CT 06520-8082

[2] Department of Physiology and Neurobiology, University of Connecticut, Storrs, Connecticut 06269

SUMMARY

Even before integrating into existing circuitry, adult-born neurons express receptors for neurotransmitters, but the intercellular mechanisms and their impact on neurogenesis remain largely unexplored. Here, we show that neuroblasts born in the postnatal subventricular zone (SVZ) acquire NMDA receptors (NMDARs) during their migration to the olfactory bulb. Along their route, neuroblasts are ensheathed by astrocyte-like cells expressing vesicular glutamate release machinery. Increasing calcium in these specialized astrocytes induced NMDAR-activity in neuroblasts and blocking astrocytic vesicular release eliminated spontaneous NMDAR-activity. Single-cell knockout of NMDARs using neonatal electroporation resulted in neuroblast apoptosis at the time of NMDAR acquisition. This cumulated in a 40% loss of neuroblasts along their migratory route demonstrating that NMDAR acquisition is critical for neuroblast survival, prior to entering a synaptic network. In addition, our findings suggest an unexpected mechanism where SVZ astrocytes use glutamate signaling through NMDARs to control the number of adult-born neurons reaching their final destination.

INTRODUCTION

Accumulating evidence suggests that the neurotransmitters GABA and glutamate are essential signaling molecules that control adult neurogenesis (Bordey, 2006; 2007; Ge et al., 2007; Platel et al., 2008a). Neurogenesis persists in two centers in the adult mammalian brain, the subventricular zone (SVZ) and the hippocampal dentate gyrus (Lledo et al., 2006; Zhao et al., 2008). In the SVZ, neural stem cells, a subpopulation of astrocyte-like cells, produce transit amplifying cells, which themselves generate neuroblasts (Doetsch et al., 1999). Neuroblasts migrate in chains ensheathed by astrocyte-like cells (also called SVZ and RMS astrocytes) throughout the SVZ and along the rostral migratory stream (RMS) to the olfactory bulb (OB) (Lois et al., 1996; Peretto et al., 1997). Once in the RMS of the OB, they turn and migrate radially to enter the existing OB circuitry and differentiate into interneurons (granule cells and periglomerular cells) (Luskin, 1993; Lois and Alvarez-Buylla, 1994).

Address for correspondence: Angélique Bordey, Ph.D., Yale Univ. Sch. Med., 333 Cedar St, FMB 422, New Haven, CT 06520-8082, Phone: 203-737-2515, Fax: 203-737-2159, angelique.bordey@yale.edu.

Prior to entering the OB circuitry, neuroblasts develop in an asynaptic environment, yet neurotransmitters seem to play a prominent role in their development. In the SVZ and RMS, GABA is released by neuroblasts to activate $GABA_A$ receptors in both neuroblasts and astrocyte-like stem cells, and then taken up by astrocyte-like cells (Stewart et al., 2002; Wang et al., 2003b; Bolteus and Bordey, 2004; Liu et al., 2005). Ultimately, GABA exerts a tonic control of the production of neuroblasts in the postnatal SVZ by limiting the proliferation of astrocyte-like stem cells (Liu et al., 2005) and neuroblasts (Nguyen et al., 2003). Glutamatergic signaling in the SVZ remains largely unexplored. SVZ and RMS neuroblasts express functional metabotropic and ionotropic AMPA/kainate-type glutamate receptors (Di Giorgi-Gerevini et al., 2005; Platel et al., 2007b; 2008b). These receptors are tonically activated and have been shown to regulate neuroblast proliferation and migration, respectively (Di Giorgi-Gerevini et al., 2005; Platel et al., 2008b). Despite the tonic activation of these receptors, the source of glutamate in the SVZ and RMS is unknown.

Here, we present surprising evidence that neuroblasts express functional NMDARs prior to entering the OB, contrary to previous work (Carleton et al., 2003). Therefore, we hypothesized that glutamate acting on NMDARs is a neurotrophic signal from SVZ/RMS astrocytes to neuroblasts en route to the OB. We tested for the presence and function of a glutamate signaling system in the postnatal SVZ/RMS using a combination of anatomical and functional approaches. We confirmed functional, activity-dependent, vesicular glutamatergic signaling from astrocyte-like cells to neuroblasts. Further, we used single-cell genetic removal of functional NMDARs in neuroblasts to examine their potential functional role in cell migration and survival. We found that NMDARs unexpectedly provide early survival cues to neuroblasts prior to entering an existing synaptic network. Glutamatergic signaling through NMDARs is, therefore, critical in controlling the number of neurons that reach the OB.

RESULTS

Neuroblasts acquire NMDARs during their migration towards the olfactory bulb

To determine whether neuroblasts express functional NMDARs in the SVZ and RMS, we obtained gramicidin-perforated patch-clamp recordings from neuroblasts in acutely dissected sagittal brain slices at near-physiological temperature (32–35°C) from mice of age postnatal day (P) 20 to 30 unless otherwise mentioned. Recorded cells were identified as neuroblasts based on their ionic signature and biophysical properties (Wang et al., 2003a; 2003b; Bolteus and Bordey, 2004) that are significantly different from the properties of SVZ astrocytes (Liu et al., 2005; 2006); neuroblasts have high input resistances (4.5 ± 0.1 GΩ, n=203) and mean depolarized zero-current resting potentials (−25 mV) while SVZ astrocytes have low input resistance (50–100 MΩ, n=26) and hyperpolarized resting potential (−80 mV). Neuroblasts were recorded in a Mg^{2+}-free solution containing 10 μM glycine to enhance NMDAR activation, and antagonists of both glycine and $GABA_A$ receptors (10 μM strychnine and 20 μM bicuculline, respectively) unless otherwise stated. Recordings were performed at different locations along the SVZ-RMS axis: along the lateral wall of the lateral ventricle (SVZ), in the rostral SVZ under the corpus callosum (rSVZ), in the RMS elbow (RMS_{EL}), and in the RMS of the OB (RMS_{OB}) where neuroblasts turn radially to enter the granule cell layer (see Figure 1H). The term RMS refers to both RMS_{EL} and RMS_{OB}. Pressure applications of NMDA (50–100 μM, 5–10 s) induced no detectable currents in neuroblasts in the SVZ (n=6, Figure 1A and 1B). However, once in the rSVZ, some neuroblasts displayed NMDA-induced inward currents (n=3/6, Figure 1A and 1B) that reversed at 0 mV (n=8, Figure 1C) and were markedly reduced by the competitive NMDAR antagonist, D-2-amino-5-phosphonovaleric acid (D-APV, n=7, see Box plot in Figure 5). Even in 3 month-old mice, pressure application of NMDA as short as 100 ms induced NMDA-channel activity in RMS_{EL} neuroblasts (n=5/7, inset in Figure 1H). In current clamp, NMDA induced depolarizations of neuroblasts were significantly and

reversibly reduced by D-2-amino-5-phosphonovaleric acid (D-APV, n=4, Figure 1D), identifying these responses as due to NMDAR activation. NMDA did not induce currents or calcium (Ca^{2+}) responses in SVZ or RMS astrocytes (n=5, Figure 1E), suggesting that these cells do not express functional NMDARs. Both the NMDA-induced charge transfer density (Q divided by the cell capacitance, C) and the percentage of recorded neuroblasts responding to NMDA (92% in the RMS_{OB}) increased significantly along the caudal to rostral axis (Figures 1B, $p<0.05$, one-way ANOVA).

To survey a larger number of neuroblasts and better determine the percentage expressing NMDARs, we used Ca^{2+} imaging in transgenic mice where Green Fluorescent Protein (GFP) is fused to a non-endogenous G-protein coupled receptor called MrgA1, only expressed in astrocytes (please see Figure 4A and B for additional information and data on these mice). As a result, GFP outlines the cell membranes of astrocytes, making them easily distinguishable from neuroblasts prior to and following loading of the Ca^{2+}-sensitive dye Fluo-4 AM (Figure 1D). In addition, an agonist of the MrgA1 receptor (the phe-leu-arg-phe amide peptide, FLRFa) increased Ca^{2+} in GFP-fluorescent cells allowing further identification of the FLRFa-responding cells as astrocytes at the end of each experiment. Recordings were performed in solution containing 0.8 mM Mg^{2+}, bicuculline, and no glycine at 33–35°C. Pressure application of NMDA (100 μM) induced transient increases in intracellular Ca^{2+} in 60% rSVZ and >85% RMS neuroblasts (n=4 to 11 recordings) but not FLRFa-responding cells, *i.e.* astrocytes (n=61 cells, Figures 1E and 1F). These Ca^{2+} responses in neuroblasts were blocked by D-APV (n=3 slices, data not shown). The percentage of neuroblasts responding to NMDA significantly increased along the caudal-rostral axis from 20% in the SVZ to 84% and 91% in the RMS_{EL} and RMS_{OB}, respectively (Figure 2G–H). Collectively, these data report an increasing expression of functional NMDARs in neuroblasts during their migration along the rSVZ and RMS.

Most RMS neuroblasts display spontaneous NMDAR-activity

We next examined whether neuroblasts display spontaneous NMDAR activation, which would suggest the presence of ambient glutamate. Neuroblasts displayed spontaneous single-channel events (sSCEs) illustrating phasic NMDAR activation (Figure 2A, same recording conditions as in Figure 1). Gaussian fit of the channel amplitude histogram for the trace partly shown in Figure 2A gave an amplitude of −3.0 pA at −64 mV (right inset in Figure 2A), resulting in a conductance of 47 pS (assuming a reversal potential of 0 mV) similar to that previously shown for NMDARs (Cull-Candy and Usowicz, 1987; Ascher et al., 1988). Neuroblasts also displayed channels with smaller amplitudes (open columns, inset in Figure 2A). To estimate SCE frequency we used a cut-off amplitude between −1.8 and −2.0 pA (depending on the noise) to measure channels with a conductance similar to that of NMDARs. The mean SCE amplitude from 9 cells averaged −2.87 ± 0.04 pA at −64 mV, giving a conductance of 45 pS (data not shown). sSCE frequency was significantly and reversibly reduced to 15.7 ± 2.8% of control by D-APV (n=23, Figure 2B), identifying most of these events as NMDAR-channel openings. As shown for NMDA-induced currents, the SCE frequency and the percentage of neuroblasts displaying sSCEs in the RMS_{EL} and RMS_{OB} (82 and 91% of the recorded neuroblasts, respectively) were significantly greater than those in the rSVZ (37%, $p<0.05$, Figure 2C and 2D).

We also examined whether phasic NMDAR activation occurred under near-physiological conditions of Mg^{2+} (0.8 mM). In voltage-clamp, sSCEs were observed in neuroblasts (2.8 ± 0.9 Hz, n=8/9 in RMS_{EL} and RMS_{OB}, data not shown). With D-APV, their frequency was reduced to 4.7 ± 2.3% of control.. In current-clamp (in 0.8 mM Mg^{2+} without bicuculline), spontaneous depolarizations in neuroblasts were reduced in amplitude and in frequency by 30–

40% during D-APV application (n=4, Figure 2E). Collectively, these data show that most neuroblasts in the RMS (>80%) receive a phasic glutamate signal via NMDAR activation.

Astrocytes of the neurogenic forebrain express machinery for vesicular release of glutamate

We previously found that SVZ and RMS astrocytes, marked by glutamate-aspartate transporter (GLAST), displayed intense glutamate staining in the SVZ (Platel et al., 2007b). Here, pre-embedding immunocytochemistry revealed that L-glutamate was concentrated in astrocytes and absent from other SVZ and RMS cells (Figure 3A). Astrocytes were identified based on their pale cytoplasm and the expression of GLAST examined on separate sections (data not shown). To determine whether SVZ astrocytes are capable of releasing glutamate in a vesicular manner, we examined the distribution of vesicular glutamate transporters (VGLUTs). The family of VGLUTs in mammals is comprised of three highly homologous proteins, VGLUT1-3. Co-immunostaining for VGLUT1, glutamate-aspartate transporter (GLAST, a marker of astrocytes, Bolteus and Bordey, 2004; Liu et al., 2006), and doublecortin (DCX, a marker of neuroblasts, Gleeson et al., 1999) revealed that only astrocytes expressed VGLUT1 (Figure 3B, Synaptic Systems antibody, Figure S1A and S1B for NeuroMab antibody). No VGLUT2 or VGLUT3 immunostaining was observed in the RMS or SVZ, while VGLUT2 and VGLUT3 staining were present in the striatum and in the hippocampus, respectively, as expected (Figure S1C and S1G). Post-embedding immunogold labeling for VGLUT1 also showed that only astrocytes contained VGLUT1 in the RMS and SVZ in electron micrographs (Figure 3C). We also immunostained for synaptobrevin 2 (also called VAMP2), a member of the v-SNARE complex that is essential for vesicular release (Sorensen, 2005). Only astrocytes (GLAST-positive cells) in the SVZ/RMS stained positive for synaptobrevin 2 (Figure 3D). In addition, co-immunostaining for VGLUT1 and synaptobrevin 2 revealed that VGLUT1 signal co-localized with synaptobrevin 2 signal (Figure S1I and S1J). However, not all synaptobrevin-2-positive puncta co-localized with VGLUT1. This latter finding was expected because SVZ astrocytes release ATP in a vesicular manner *in vitro* (Striedinger et al., 2007), and not all vesicles are readily releasable. While VGLUT1 and synaptobrevin-2 are expressed in neurons and in some mature astrocytes (Montana et al., 2004; Bezzi et al., 2004; Zhang et al., 2004; Boulland et al., 2004), they are only expressed in astrocytes in the SVZ and RMS. The lack of VGLUT1 and synaptobrevin-2 in neuroblasts was expected because they synthesize and release GABA in a non-vesicular mechanism (Liu et al., 2005). These data suggest that SVZ/RMS astrocytes may be a source of glutamate, likely releasing it in a vesicular and potentially Ca^{2+}-dependent manner.

Calcium increases in RMS astrocytes lead to NMDAR activity in neuroblasts

We next explored whether RMS astrocytes release glutamate in a Ca^{2+}-dependent manner resulting in NMDAR activation in neuroblasts. We used transgenic mice that express a Gq-protein coupled receptor (called Mas-related gene A1, MrgA1) in astrocytes to evoke Ca^{2+} increases using the peptide agonist FLRFa that does not bind endogenous receptors in the brain (Fiacco et al., 2007). The MrgA1 receptor fused to GFP was targeted to astrocytes using the inducible tet-off system. Mice expressing the tetracycline transactivator (tTA) under the human *glial fibrillary acidic protein (GFAP)* promoter were crossed to mice in which the MrgA1 receptor was transcribed off the tet (tetO) minimal promoter. In the SVZ of *hGFAP*-tTA x tetO-MrgA1 mice (referred henceforth as $MrgA1^+$ mice), GFP fused to MrgA1 is selectively expressed in SVZ astrocytes that are identified by GFAP and brain lipid-binding protein (BLBP) staining (Platel et al., 2009) (Figure 4A). GFP was not in DCX-immunopositive cells, *i.e.* neuroblasts (Figure S2A and S2B). Pressure application of FLRFa (5 μM, 10 s) induced intracellular Ca^{2+} increases in Fluo-4-loaded cells that express MrgA1-GFP (Figure 4B, movie S1). These data confirmed the $MrgA1^+$ mouse line as a viable tool for selective stimulation of SVZ/RMS astrocytes, similar to the previous report in the hippocampus (Fiacco et al., 2007).

We examined the effects of astrocytic stimulation by FLRFa on baseline NMDA-channel activity in neuroblasts in acute sagittal slices from MrgA1^{+} mice at 32–35°C (see Figure 4C top for diagram). Using gramicidin-perforated patch clamp recordings, tonic SCE frequency in RMS neuroblasts was significantly increased to 312 ± 35% of control upon bath application (5 μM, 60 s) of FLRFa (n=9, $p<0.01$, Figure 4C and 4D). FLRFa did not induce a detectable change in channel amplitude (data not shown). The FLRFa-induced increase in channel activity was significantly reduced to 18 ± 5% of control by addition of 50 μM D-APV (n=7, $p<0.01$, Figure 4C and 4D), identifying most of this activity as NMDAR-mediated. In single transgenic mice (expressing only the tetO-MrgA1 construct, MrgA1^{-} mice) FLRFa did not significantly increase SCE frequency (112% of control with FLRFa) although these neuroblasts showed D-APV-sensitive activity (19% of control in D-APV, n=4, Figure 4D). These control experiments show the effectiveness of the tet-off system in targeting MrgA1 to astrocytes and that FLRFa does not directly increase the frequency of NMDA receptor activity. Collectively, these data suggest that selective intracellular Ca^{2+} increases in RMS astrocytes lead to glutamate release that activates NMDARs in neuroblasts.

Vesicular release of glutamate from astrocytes controls NMDAR activity in neuroblasts

To determine whether a vesicular pathway was involved in glutamate release, we perturbed two critical processes in the vesicular release pathway. First, we blocked vesicular re-filling using the vacuolar H^{+}-ATPase inhibitor, concanamycin A (Drose et al., 1993). Concanamycin A (5 μM, 4–5 hr preincubation) eliminated sSCEs (n=5 cells, Figure 4G and traces in Figure S2C). In addition, neuroblasts pre-treated with concanamycin A still displayed NMDA-induced currents induced by pressure application of NMDA (Figure S2C) indicating that concanamycin A did not directly interfere with NMDARs. Second, we used two *Clostridium botulinum* neurotoxins (BoNT), A and B. BoNT/A cleaves the t-SNARE complex protein SNAP-25 in neurons and BoNT/B cleaves the v-SNARE complex protein synaptobrevin 2 in neurons and astrocytes (Araque et al., 2000; Schiavo et al., 2000). Acute slices were incubated for 15–20 hrs at room temperature in control artificial cerebrospinal fluid (aCSF) or aCSF containing 200 nM of either toxin. Neuroblasts in the RMS_{OB} of sagittal slices incubated for 10–20 hrs in control aCSF displayed channel activity at a frequency of 3.3 ± 0.8 Hz (n=6) that was significantly reduced by D-APV (traces not shown, but see Figure 4G). Incubation in BoNT/A did not significantly decrease SCE frequency in neuroblasts (3.1 ± 0.7 Hz, n=5 compared to 3.3 Hz in control aCSF, Figure 4E and 4G). D-APV significantly reduced channel activity in BoNT/A-incubated neuroblasts (0.6 ± 0.3 Hz, n=5), identifying this activity as mostly mediated by NMDARs. As a control, neurons in BoNT/A treated slices did not display spontaneous excitatory synaptic currents (n=6/6, data not shown). However, incubation in BoNT/B resulted in a complete block of tonic NMDAR-channel activity in neuroblasts (n=6, Figure 4F and 4G). This effect was not a direct blockade of NMDA receptors because NMDA application (10 μM) induced inward currents in neuroblasts (n=4/4, Figure S2D). Collectively, these data suggest that intracellular Ca^{2+}-dependent vesicular fusion in astrocytes of the neurogenic forebrain contributes to glutamate release and NMDAR activation in migrating neuroblasts.

Single-cell knockout of functional NMDARs in neuroblasts using *in vivo* postnatal electroporation

To explore the role of NMDAR in neurogenesis we genetically removed NMDARs in individual neuroblasts using *in vivo* electroporation in neonatal mice (Boutin et al., 2008; Chesler et al., 2008). We used transgenic NR1$^{fl/fl}$ mice crossed with Rosa26-STOP-YFP reporter mice to generate NR1^{fl}/R26R-YFP mice (Y for yellow and fl for floxed). In NR1^{fl} mice the gene encoding the NMDAR subunit NR1, which is essential for NMDAR functionality, is flanked by loxP sites (i.e. floxed, fl, diagram in Figure 5A). In R26R-YFP mice a STOP sequence is flanked by loxP sites preventing YFP expression. Expression of Cre

recombinase (Cre) in cells of R26R-YFP/NR1^{fl} mice is expected to excise the STOP sequence and a portion of the NR1 gene, resulting in YFP expression and loss of functional NMDARs in Cre-containing cells.

To express Cre in neuroblasts, we electroporated a Cre-containing plasmid into SVZ cells of R26R-YFP mice (controls) and R26R-YFP/NR1^{fl} mice at postnatal day (P) 1 (Figure 5A and 5B for diagram). In R26R-YFP mice, this method resulted in permanent YFP expression in SVZ cells, including neural progenitor cells anchored in the SVZ (Platel et al., 2009). Since neural progenitors continuously generate neuroblasts during postnatal life, YFP$^+$ neuroblasts are continuously born over time and accumulate in the OB (Figure 5C and 5D). It takes 7–11 days for neuroblasts born in the SVZ to reach the RMS$_{OB}$ (data not shown). At 7 days post-electroporation up to 2 months (last time point examined), we found that approximately 20% of neuroblasts were YFP$^+$ cells in the RMS (Figure 5D for 2 weeks). By 2 weeks post-electroporation, YFP$^+$ neurons were found in the granule cell layer (Figure 5C).

To assess the functional knockout (KO) of NR1 by Cre recombination, we used both patch clamp recordings and Ca^{2+} imaging to examine the loss of functional NMDARs in neuroblasts. Both patch clamp recordings and Ca^{2+} imaging were performed as described in Figure 1. YFP$^+$ cells were identified prior to recordings or Fluo-4 AM loading and were neuroblasts as shown in Figure 5D (DCX positive). In the RMB$_{OB}$ from R26R-YFP/NR1^{fl} mice (acute slices), pressure applications of NMDA (100 μM, 5–10 s) induced no detectable currents in YFP$^+$ neuroblasts (n=11/11, Figure 5F), but NMDA induced currents in surrounding YFP-negative neuroblasts (n=8/11) in the same slices (data not shown). Furthermore, in R26R-YFP control mice, application of NMDA induced currents in YFP-positive neuroblasts (n=9/11, Figure 5E). Using Ca^{2+} imaging in slices from R26R-YFP/NR1^{fl} mice, 97% of the YFP$^+$ neuroblasts did not respond to NMDA (109/113), but NMDA induced Ca^{2+} increases in surrounding YFP-negative cells as expected based on the electrophysiology data (12 recordings, Figure 5G and 5I). In addition, 87% of YFP$^+$ neuroblasts in control slices from R26R-YFP mice responded to NMDA application (n=36 cells, 9 recordings, Figure 5H and 5I). These data show that the YFP fluorescence did not mask Ca^{2+} increases induced by NMDA and that electroporation and Cre expression has no effect on the expression of NMDARs.

These data show that *in vivo* electroporation of a Cre-containing plasmid into SVZ cells of R26R-YFP/NR1^{fl} mice resulted in knockout of NR1 and loss of functional NMDARs in single neuroblasts born throughout postnatal life.

NMDAR does not regulate neuroblast migration

We have previously monitored neuroblast migration in acute tissue using DIC or fluorescence visualization of GFP-expressing neuroblasts in *DCX*-GFP transgenic mice (Bolteus and Bordey, 2004; Platel et al., 2008b). Here the fact that 20–30% of RMS neuroblasts were YFP-positive allowed us to easily distinguish and track the same migrating neuroblasts in acute slices using time-lapse imaging (Figure 6A). The following experiments were performed at P25–P30 (4th week post-electroporation) as for most of the electrophysiology and Ca^{2+} imaging data.

We first examined whether genetic removal of NMDARs in RMS neuroblasts would affect their speed of migration. We found that YFP$^+$ neuroblasts migrated at similar speed in acute slices from both R26R-YFP and R26R-YFP/NR1^{fl} mice (62.2 ± 2 μm/hr and 64.2 ± 2.7 μm/hrs, respectively, n=227 cells, 6 mice, and n=100 cells, 3 mice, Figure 6B, movie S2). Next, we examined the effect of 50 μM D-APV or 10 μM NMDA on the speed of RMS neuroblast migration in control R26-YFP mice. YFP$^+$ neuroblasts in such mice express functional NMDARs (see Figure 5E and 5H). In addition, NMDA pressure applied at 10 μM was sufficient to induce inward current in RMS neuroblasts (Figure S2C). During a 1 hr control movie,

neuroblasts in the RMS migrated at 66.3 ± 2.4 μm/h (n=6 slices) and displayed classical saltatory movement (Movie S3 and S4). Bath application of 10 μM NMDA or 50 μM D-APV did not affect the speed of migration of YFP^+ neuroblasts (Figure 6A and 6B, n>15 cells per slice, same cells tracked under control and during treatment, 3 slices per condition). Therefore, genetic or pharmacological manipulations of NMDARs did not affect the speed of neuroblast migration.

In vivo blockade and genetic removal of NMDARs decrease neuroblast survival

NMDARs have recently been shown to prevent apoptosis of adult-born granule neurons during their synaptic integration into the hippocampal network (Tashiro et al., 2006). To examine whether NMDAR activity controls the survival of neuroblasts during their migration and before integration into the OB, we first injected a NMDAR blockers *in vivo*. Mice expressing GFP under the *DCX* promoter (*DCX*-GFP) mice received a single injection of the NMDAR open-channel blocker, MK-801 (1 mg/kg). At different time points (2, 6, and 24 hrs) following injection, staining for activated caspase 3 (a marker of apoptotic cells) was performed in sagittal slices to examine the number of apoptotic neuroblasts (Figure 7A).

Quantification of the density of activated caspase 3-positive neuroblasts (cell number divided by the volume) indicates that blockade of NMDARs resulted in a significant >2-fold increase in the density of apoptotic neuroblasts in the rSVZ at 6 hr post-MK801 injection (n=4 mice per condition, $p<0.05$, Figures 7B). The number of apoptotic cells returned to control levels by 24 hrs in the rSVZ. In the RMS_{EL} blockade of NMDARs resulted in a significant >2-fold increase in the density of apoptotic neuroblasts at each time point with a peak at 6 hrs (Figures 7B). This result is consistent with the presence of neuroblasts with relatively high NMDAR-channel frequency in the RMS (2–11 Hz) compared to the lower frequency in the rSVZ (<2 Hz, see Figure 2C and diagram in Figure 7D). These data suggest that NMDAR activation is an important survival cue for neuroblasts migrating within the asynaptic environments of the RMS, before their integration in the synaptic circuitry of the OB.

To next assess whether genetic removal of NMDARs selectively in neuroblasts resulted in increased apoptosis, we immunostained sagittal sections for activated caspase 3 and DCX in electroporated control (R26R-YFP) and R26R-YFP/$NR1^{fl}$ mice. The percentage of apoptotic YFP^+ neuroblasts was calculated out of the total number of YFP^+ neuroblasts. This percentage was obtained at the 4^{th} week post-electroporation time-point and at two additional time-points (2 and 8 weeks post-electroporation) corresponding to the end of the neonatal period and young adult age. In addition, apoptosis was examined in the rSVZ, the RMS, and the granule cell layer of the OB. We found that the percentage of activated caspase 3^+ YFP^+ neuroblasts was significantly increased in the rSVZ and RMS at each time-point ($p<0.05$, Figure 7C). There was also a significant increase in apoptosis of NR1-KO neurons in the granule cell layer at 4 and 8 weeks ($p<0.05$). This increase in the number of apoptotic neuroblasts is unlikely to be due to Cre toxicity since control mice (R26-YFP) also received a Cre containing plasmid.

These data suggest that acquisition of NMDARs in neuroblasts, which occurs along the rSVZ and to a lesser extent in the RMS_{EL} (Figure 7D), is critical for their survival during their migration to the OB. In addition, such an increase in the percentage of apoptotic neuroblasts from less than 0.1% to 1–3% following NR1 knockout suggests a significant reduction in the number of neuroblasts reaching the OB. Indeed, considering the estimate that ~10,000 neuroblasts are born per day, ~200 NR1-KO neuroblasts (1–3%) will be apoptotic (activated caspase-3^+) and then cleared in ~1 day. Since its takes ~11 days for all newly born neuroblasts to migrate from the SVZ to the RMS_{OB}, apoptosis would result in a cumulated loss of ~2,200 neuroblasts in the RMS_{OB}, which corresponds to 22% of the original neuroblast population. This is a conservative estimate because activated caspase-3^+ cells may be detectable for less than 24 hrs, therefore underestimating the percentage of apoptotic cells. To confirm this

estimate, we next quantified the number of YFP^+ neuroblasts along the SVZ-RMS axis and in the OB.

Genetic removal of functional NMDA receptors results in decreased neurogenesis

The density of YFP-expressing neuroblasts in the early rSVZ revealed that there was no significant difference in electroporation efficiency (Figure 8A and 8B, cell count normalized by the area). In addition, these data suggest that there is no defect in SVZ astrocyte-like stem cells giving rise to transit amplifying cells that generate neuroblasts. In contrast, cell counting revealed that there was a significant decrease in the density of YFP-expressing neuroblasts in the RMS of $NR1^{fl}$/R26R-YFP mice (red bars) compared to control mice (black bars) at every time-point (25–35% decrease, $p<0.05$, Figure 8A and 8B). The ratio of the cell density in the $NR1^{fl}$/R26R-YFP mice over those in R26R-YFP mice gave a 25 to 35% decrease in the number of NR1-KO neuroblasts that reach the RMS (Figure 8C). In the RMS, neuroblasts are in transit to the OB and accumulate in the granule cell layer. It is thus not surprising that cell loss in the RMS was accompanied by a significant decrease (>40%) in the density of YFP-expressing neurons in the granule cell layer at every time point culminating to ~65% decrease at 8 weeks. Collectively, these data show that genetic removal of NMDARs in neuroblasts results in apoptosis during their migration to the OB prior to synaptic integration, and thus, a significant reduction in neurogenesis. Therefore, signaling via NMDARs provides an important in vivo survival cue for neuroblasts even before they assume their roles as interneurons in the OB circuitry.

DISCUSSION

We show here that Ca^{2+} activity in SVZ/RMS astrocytes governs glutamate signaling in the neurogenic forebrain and induces phasic NMDAR activation in neuroblasts in the absence of synapses. We also identify a primary role of this signaling in early survival of migrating neuroblasts through NMDARs. Genetic removal of NMDARs in neuroblasts leads to the death of more than one third of the neuroblasts born in the young adult brain, prior to entering a synaptic network.

Neuroblasts acquire NMDARs during migration in the rSVZ and most neuroblasts display spontaneous NMDAR-channel activity in the RMS

Our data from patch clamp experiments show that neuroblasts express functional NMDARs earlier than previously thought (Carleton et al., 2003), but are consistent with the presence of functional NMDA receptors in neurosphere cultures from the perinatal SVZ (Brazel et al., 2005). Carleton et al. (2003) did not observe NMDA-induced currents in RMS_{OB} neuroblasts presumably because neuroblasts were recorded in the whole cell configuration, resulting in rundown of NMDA-currents (Legendre et al., 1993). Here, we used the perforated patch clamp technique to keep the intracellular medium as intact as possible. We obtained relatively long recordings (>30 min) with stable NMDAR-mediated currents during the entire duration of recording. Recorded neuroblasts did not display functional NMDARs in the SVZ (i.e. along the lateral ventricle) although NR1 expression was observed in SVZ neuroblasts (Nacher et al., 2007). Rather, neuroblasts acquire functional NMDARs during their tangential migration in the rSVZ and ~80% of neuroblasts display functional NMDARs as early as in the RMS_{EL}. Experiments using genetic removal of functional NMDARs provide strong evidence that NMDA-induced currents were due to direct NMDAR activation in the recorded neuroblasts. We also found that the density of NMDARs increased in neuroblasts migrating along the RMS, suggesting that neuroblasts undergo a progressive differentiation, perhaps being primed to integrate into the OB synaptic network. During development the NR2B subunit is the first to be expressed (Monyer et al., 1994); future studies will be required to determine the subunit composition of NMDARs in neuroblasts of the SVZ and RMS.

Neuroblasts also displayed spontaneous single-channel events sensitive to D-APV, identifying them as NMDAR-mediated events. Intriguingly, NMDAR-channel activity was observed in the presence of a physiological Mg^{2+} concentration, suggesting that these channels may have a low sensitivity to voltage-dependent Mg^{2+} blockade. Future identification of the subunit composition will shed light on the Mg^{2+} sensitivity.

Activity-dependent astrocyte-to-neuroblast glutamate signaling in the SVZ and RMS

The presence of spontaneous NMDAR activity in neuroblasts suggests a phasic release of glutamate in the RMS. Our immunostaining data indicate that RMS astrocytes, but not neuroblasts, express VGLUT1 and synaptobrevin-2, and may thus be a source of vesicular glutamate. In addition, electron micrographs illustrated VGLUT1 nanogold particles on structures resembling vesicles (including fusing vesicles) in astrocytes. Consistent with this finding, selective Ca^{2+} increase in RMS astrocytes in $MrgA1^{+}$ mice induced glutamate release resulting in NMDAR activation in surrounding neuroblasts. This finding is remarkable considering that selective Ca^{2+} increase in mature astrocytes has failed to result in receptor activation in neurons in the hippocampus (Fiacco et al., 2007). Such findings highlight the differences between regions predominated by asynaptic versus synaptic signaling. Consistent with VGLUT1 presence in SVZ/RMS astrocytes, data obtained with BoNT treatments suggest that vesicular release of glutamate from RMS astrocytes contributes to the phasic NMDAR activity in migrating neuroblasts. Indeed, blocking only neuronal release did not significantly affect NMDAR activity, while blocking both neuronal and astrocytic glutamate release with BoNT/B abolished NMDAR activity in neuroblasts. These data suggest a minor or no contribution from neuronal vesicular release to ambient glutamate level in the SVZ/RMS milieu. Therefore, our functional data are consistent with previous anatomical reports of a lack of axon terminals in the RMS (Lois et al., 1996). The next step in elucidating intercellular signaling that regulates neurogenesis will be to investigate which signals control Ca^{2+} activity in SVZ/RMS astrocytes and thus regulate glutamate release. For example, unpublished data from our lab suggest that GABA and prostaglandin E2 induce Ca^{2+} increases in RMS astrocytes. It was also reported that $GABA_A$Rs are tonically activated in RMS astrocytes and that blocking them results in a decrease in spontaneous Ca^{2+} activity in SVZ astrocytes (Liu et al., 2005; Snapyan et al., 2009). Collectively, our findings suggest that RMS astrocytes in the neurogenic zone are the major source of glutamate that contributes to phasic NMDAR activity in migrating neuroblasts.

Function of glutamatergic signaling on olfactory bulb neurogenesis

Our data suggest that in the SVZ-to-RMS axis, NMDARs do not control the migration, but are important for the survival of neuroblasts. Pharmacologically blocking or activating NMDARs in acute slices did not affect the speed of neuroblast migration. Similarly, NR1-KO neuroblasts migrated at the same speed as control neuroblasts in acute slices. These results differ from findings in the neonatal cerebellum, where NMDARs tonically enhance the speed of granule cell precursor migration (Komuro and Rakic, 1993) and cortical progenitors (Behar et al., 1999), but is consistent with the Ca^{2+}-independence of RMS neuroblast migration in the RMS_{OB} (Darcy and Isaacson, 2009).

Our main finding regarding apoptosis is that expression of functional NMDARs is critical for neuroblast survival during the long-distance migration from the SVZ to the RMS_{OB}. This is a new and critical function of NMDARs in immature neurons prior to their entry into a synaptic network. Blockade of NMDARs *in vivo* resulted in a significant increase of apoptotic neuroblasts in the RMS where phasic NMDAR activation by ambient glutamate is higher compared to that in the rSVZ. Genetic NR1 removal and thus loss of functional NMDARs at the time of neuroblast birth resulted in apoptosis all along the rSVZ and RMS. These data suggest that a large proportion of neuroblasts that did not acquire NMDARs underwent

apoptosis. Some NR1-KO neuroblasts escaped apoptosis possibly due to compensation through other glutamate receptors (Platel et al., 2007b; 2008b). Alternatively, it is possible that only a subtype of adult born neurons was affected by NMDAR removal. In addition to deficits in granule cells there was a significant 54% decrease in the density of periglomerular cells in $NR1^{fl}$ mice compared to control mice at 4 weeks (Platel JC and Bordey A, unpublished observation). Nevertheless, it is important to determine whether subpopulations of granule and periglomerular cells or glutamatergic neurons are selectively affected by NMDAR removal (Brill et al., 2009). Regarding the density data, it is intriguing that apoptosis at 2 weeks post-electroporation is less than at 4 or 8 weeks. This may be due to the different cellular organization of the SVZ in neonates versus older mice (Peretto et al., 1997); neonates have a single chain of neuroblasts instead of multiple chains each ensheathed by astrocytes in older animals. As a result, the distance between neuroblasts to astrocytes is greater in neonatal tissue than in older tissue and NMDAR may be less activated by ambient glutamate.

The other finding not highlighted in the results is the significant increase in the number of apoptotic NR1-KO neurons in the granule cell layer compared to control neurons. These data match findings from previous studies in the perinatal cortex and the adult hippocampal neurogenic zone. It was reported that NMDA promotes the survival of neurons during synaptic integration in the perinatal cortex (Ikonomidou et al., 1999) and in the adult hippocampal granule cell layer (Tashiro et al., 2006). One outcome predicted by the increased apoptosis is a decreased number of newly-born neuroblasts and neurons. Indeed, cell counting highlighted a significant cell loss in the RMS and granule cell layer. The decrease in the number of neuroblasts was between 30–40% at 4 and 8 weeks in the RMS. We cannot rule out that other developmental defects (e.g. proliferation (Gould et al., 1994; Cameron et al., 1995; Petrus et al., 2009)) contribute to the decrease in cell number. Nevertheless, removal of NMDARs resulted in a significant decrease in neonatal and adult neurogenesis.

In conclusion, astrocyte-to-neuroblast glutamate signaling in the neurogenic SVZ/RMS region controls NMDAR activity in neuroblasts. This glutamatergic signal through NMDARs critically controls the number of neurons that ultimately reach the olfactory bulb and are available to integrate into the existing synaptic network. These data suggest that acquisition of NMDARs en route to their final destination is necessary for proper genetic programming of cell survival and ongoing development.

EXPERIMENTAL PROCEDURES

Mice and acute slice preparation

Experiments were performed in CD1 mice (Charles River Laboratories) and transgenic mice: *DCX*-GFP (gift from Dr. R. Miller, University of Chicago, Gensat), Rosa26-STOP-YFP (R26R-YFP), R26R-YFP crossed with $NR1^{fl/fl}$ mice (R26R-YFP/$NR1^{fl}$), *hGFAP*-GFP (Jackson labs), and *hGFAP*-tTA crossed with *TetO*-MrgA1 mice (gift from Dr. Ken McCarthy, University of North Carolina at Chapel Hill). Experiments were performed at postnatal day (P) 19 to 30 in >3 mice unless otherwise noted (*e.g. in vivo* experiments performed in >4 mice up to 8 weeks old). Acute sagittal slices containing the SVZ and RMS were prepared as previously described (Bolteus and Bordey, 2004, see Supplemental Material). All experiments were in accordance with protocols approved by the Yale Animal Care and Use Committee.

Electrophysiology

Neuroblasts were recorded in sagittal sections using the gramicidin perforated patch-clamp technique as previously described (Wang et al., 2003b) (see Supplemental Material). The recording aCSF contained (in mM): 126 NaCl, 2.5 KCl, 2 $CaCl_2$, 1.25 NaH_2PO_4, 24 $NaHCO_3$, 10 glucose, and (in μM) 10 glycine, 20 bicuculline and 10 strychnine (unless

otherwise mentioned), pH 7.4 when equilibrated with 95% O_2/5% CO_2. The internal solution contained (in mM): 125 CsCl, 10 Hepes, 6 $MgCl_2$, 2 EGTA, 0.1 $BaCl_2$; pH 7.3, 295–300 mOsmol. Single channel data were analyzed for frequency using the single channel and threshold detection functions in Clampfit 9 (Axon Instruments). The threshold amplitude was set between −1.8 and −2 pA.

Calcium imaging

Cells were pressure loaded with Fluo-4 AM (1–2 min, 125 μM in DMSO with 20% Pluronic acid F-127). Ca^{2+} imaging experiments were performed on an Olympus Fluoview 1000 confocal microscope equipped with 60× objective (NA 0.9, WD 2 mm). Analysis of Ca^{2+} data was performed in >4 slices from >3 mice with Calsignal (Platel et al., 2007a). F_0 and F are the mean fluorescence intensity measured through all the regions of interest and in a single cell, respectively. A change in fluorescence was considered to be a Ca^{2+} increase if F/F_0>20%.

Immunohistochemistry

Immunostaining performed in free-floating 100 μm-thick slices was as previously described (Platel et al., 2009). The primary antibodies included: rabbit anti-GFAP (1:1000, Dako), goat anti-DCX (1:100, Santa Cruz), chicken anti-GFP (1:500, Abcam), guinea pig anti-GLAST (1:500, Chemicon, USA), mouse anti-synaptobrevin 2 (1:100), rabbit anti-VGLUT1, 2, or 3 (1:1000, Synaptic Systems and NeuroMab), and rabbit anti-activated caspase 3 (1:500, Cell Signaling Technology).

Pre-embedding immunocytochemistry for L-glutamate and Post-embedding immunogold labeling for VGLUT1

These methods were as previously described (Rubio and Wenthold, 1999; Rubio and Juiz, 2004) (see Supplemental Material).

NMDAR blockade *in vivo*

P20-30 *DCX*-GFP transgenic mice received a single intraperitoneal injection of 100 μl saline (control) or 100 μl of saline solution containing 1 mg/kg body weight of MK-801. Mice were sacrificed 2, 6, or 24 hours after the injection as described above (n=4 mice per time-point per condition).

Postnatal *in vivo* electroporation

A pCAG-Cre:GFP plasmid (5 μg/μl, Addgene, Matsuda and Cepko, 2007) was diluted in PBS containing 0.1% fast green as a tracer. 0.5–1 μl of plasmid solution was injected into the lateral ventricle using a pulled glass pipette (beveled to a <50 μm diameter) in pups anesthetized on ice. After plasmid injection using manual pressure, tweezer-type electrodes (model 520, BTX) were placed on the heads of the P0–P1 pups, and 5 square-pulses of 50-ms duration with 950-ms intervals at 150V were applied using a pulse ECM830 BTX generator.

Neuroblast migration

R26R-YFP mice (P20-30) that received Cre -containing plasmids at P1 (electroporation) were used for examining neuroblast migration. Migration movies were acquired at 37°C on the Olympus confocal microscope with a Super 20× objective (NA 0.95) in high glucose DMEM using acute sagittal slices as previously described (Platel et al., 2008b) (see Supplemental Material).

Neuroblast count

Dissected brains were fixed in 4% paraformaldehyde to prepare 100 μm-thick sections. For quantifying the number of apoptotic neuroblasts, the number of activated caspase 3^+ cells that were GFP^+ cells (in *DCX*-GFP mice) or DCX^+/YFP^+ cells was counted in sagittal sections in control and MK-801 injected mice, or R26R-YFP and R26R-YFP/$NR1^{fl}$ mice, respectively. The number of YFP^+/caspase 3^+ neuroblasts was divided by the total number of YFP^+ neuroblasts to yield a % of apoptotic neuroblasts. For quantifying cell density, the number of DCX^+/YFP^+ cells was counted in sagittal sections in R26R-YFP and R26R-YFP/$NR1^{fl}$ mice. Confocal z-stacks (2 μm-spaced 3–10 sections) of 3 square fields of view were obtained per region using a 20x objective (NA, 0.75). Cell number divided by volume yielded cell density. In Figure 8C, the cell density was normalized by the number of YFP^+ neuroblasts in the rSVZ yielding a normalized cell density. The latter normalization was performed to correct for slight variation introduced by variability in electroporation efficiency. Nevertheless, cell density in the rSVZ was not significantly different.

Drugs

(see Supplemental Material)

Statistical analysis

Statistical significance was determined using the two-tailed Student's t-test ($p<0.05$) unless otherwise noted. Data are presented as mean ± standard error of the mean (SEM).

Supplementary Material

Refer to Web version on PubMed Central for supplementary material.

Acknowledgments

We thank K.E. Gipson and members of the Bordey lab for their comments. This work was supported by grants from the NIH (NS042189 and NS048256; A.B.) and National Science Foundation Graduate Research Fellowships (K.A.D. and B.L.).

References

Araque A, Li N, Doyle RT, Haydon PG. SNARE protein-dependent glutamate release from astrocytes. J Neurosci 2000;20:666–673. [PubMed: 10632596]

Ascher P, Bregestovski P, Nowak L. N-methyl-D-aspartate-activated channels of mouse central neurones in magnesium-free solutions. J Physiol 1988;399:207–226. [PubMed: 2457087]

Behar TN, Scott CA, Greene CL, Wen X, Smith SV, Maric D, Liu QY, Colton CA, Barker JL. Glutamate acting at NMDA receptors stimulates embryonic cortical neuronal migration. J Neurosci 1999;19:4449–4461. [PubMed: 10341246]

Bezzi P, Gundersen V, Galbete JL, Seifert G, Steinhauser C, Pilati E, Volterra A. Astrocytes contain a vesicular compartment that is competent for regulated exocytosis of glutamate. Nat Neurosci 2004;7:613–620. [PubMed: 15156145]

Bolteus AJ, Bordey A. GABA Release and Uptake Regulate Neuronal Precursor Migration in the Postnatal Subventricular Zone. J Neurosci 2004;24:7623–7631. [PubMed: 15342728]

Bordey A. Adult Neurogenesis: Basic Concepts of Signaling. Cell Cycle 2006;5:722–728. [PubMed: 16582623]

Bordey A. Enigmatic GABAergic networks in adult neurogenic zones. Brain Res Brain Res Rev 2007;53:124–134.

Boulland JL, Qureshi T, Seal RP, Rafiki A, Gundersen V, Bergersen LH, Fremeau RT Jr, Edwards RH, Storm-Mathisen J, Chaudhry FA. Expression of the vesicular glutamate transporters during

development indicates the widespread corelease of multiple neurotransmitters. J Comp Neurol 2004;480:264–280. [PubMed: 15515175]

Boutin C, Diestel S, Desoeuvre A, Tiveron MC, Cremer H. Efficient in vivo electroporation of the postnatal rodent forebrain. PLoS ONE 2008;3:e1883. [PubMed: 18382666]

Brazel CY, Nunez JL, Yang Z, Levison SW. Glutamate enhances survival and proliferation of neural progenitors derived from the subventricular zone. Neuroscience 2005;131:55–65. [PubMed: 15680691]

Brill MS, Ninkovic J, Winpenny E, Hodge RD, Ozen I, Yang R, Lepier A, Gascon S, Erdelyi F, Szabo G, Parras C, Guillemot F, Frotscher M, Berninger B, Hevner RF, Raineteau O, Gotz M. Adult generation of glutamatergic olfactory bulb interneurons. Nat Neurosci 2009;12:1524–1533. [PubMed: 19881504]

Cameron HA, McEwen BS, Gould E. Regulation of adult neurogenesis by excitatory input and NMDA receptor activation in the dentate gyrus. J Neurosci 1995;15:4687–4692. [PubMed: 7790933]

Carleton A, Petreanu LT, Lansford R, Alvarez-Buylla A, Lledo PM. Becoming a new neuron in the adult olfactory bulb. Nat Neurosci 2003;6:507–518. [PubMed: 12704391]

Chesler AT, Le Pichon CE, Brann JH, Araneda RC, Zou DJ, Firestein S. Selective gene expression by postnatal electroporation during olfactory interneuron nurogenesis. PLoS ONE 2008;3:e1517. [PubMed: 18231603]

Cull-Candy SG, Usowicz MM. Multiple-conductance channels activated by excitatory amino acids in cerebellar neurons. Nature 1987;325:525–528. [PubMed: 2433594]

Darcy DP, Isaacson JS. L-type calcium channels govern calcium signaling in migrating newborn neurons in the postnatal olfactory bulb. J Neurosci 2009;29:2510–2518. [PubMed: 19244525]

Di Giorgi-Gerevini V, Melchiorri D, Battaglia G, Ricci-Vitiani L, Ciceroni C, Busceti CL, Biagioni F, Iacovelli L, Canudas AM, Parati E, De Maria R, Nicoletti F. Endogenous activation of metabotropic glutamate receptors supports the proliferation and survival of neural progenitor cells. Cell Death Differ 2005;12:1124–1133. [PubMed: 15947794]

Doetsch F, Caille I, Lim DA, Garcia-Verdugo JM, Alvarez-Buylla A. Subventricular zone astrocytes are neural stem cells in the adult mammalian brain. Cell 1999;97:703–716. [PubMed: 10380923]

Drose S, Bindseil KU, Bowman EJ, Siebers A, Zeeck A, Altendorf K. Inhibitory effect of modified bafilomycins and concanamycins on P- and V-type adenosinetriphosphatases. Biochemistry 1993;32:3902–3906. [PubMed: 8385991]

Fiacco TA, Agulhon C, Taves SR, Petravicz J, Casper KB, Dong X, Chen J, McCarthy KD. Selective stimulation of astrocyte calcium in situ does not affect neuronal excitatory synaptic activity. Neuron 2007;54:611–626. [PubMed: 17521573]

Ge S, Pradhan DA, Ming GL, Song H. GABA sets the tempo for activity-dependent adult neurogenesis. Trends Neurosci 2007;30:1–8. [PubMed: 17116335]

Gleeson JG, Lin PT, Flanagan LA, Walsh CA. Doublecortin is a microtubule-associated protein and is expressed widely by migrating neurons. Neuron 1999;23:257–271. [PubMed: 10399933]

Gould E, Cameron HA, McEwen BS. Blockade of NMDA receptors increases cell death and birth in the developing rat dentate gyrus. J Comp Neurol 1994;340:551–565. [PubMed: 7911808]

Ikonomidou C, Bosch F, Miksa M, Bittigau P, Vockler J, Dikranian K, Tenkova TI, Stefovska V, Turski L, Olney JW. Blockade of NMDA receptors and apoptotic neurodegeneration in the developing brain. Science 1999;283:70–74. [PubMed: 9872743]

Komuro H, Rakic P. Modulation of neuronal migration by NMDA receptors. Science 1993;260:95–97. [PubMed: 8096653]

Legendre P, Rosenmund C, Westbrook GL. Inactivation of NMDA channels in cultured hippocampal neurons by intracellular calcium. J Neurosci 1993;13:674–684. [PubMed: 7678859]

Liu X, Bolteus AJ, Balkin DM, Henschel O, Bordey A. GFAP-expressing cells in the postnatal subventricular zone display a unique glial phenotype intermediate between radial glia and astrocytes. Glia 2006;54:394–410. [PubMed: 16886203]

Liu X, Wang Q, Haydar TF, Bordey A. Nonsynaptic GABA signaling in postnatal subventricular zone controls proliferation of GFAP-expressing progenitors. Nat Neurosci 2005;8:1179–1187. [PubMed: 16116450]

Lledo PM, Alonso M, Grubb MS. Adult neurogenesis and functional plasticity in neuronal circuits. Nat Rev Neurosci 2006;7:179–193. [PubMed: 16495940]

Lois C, Alvarez-Buylla A. Long-distance neuronal migration in the adult mammalian brain. Science 1994;264:1145–1148. [PubMed: 8178174]

Lois C, Garcia-Verdugo JM, Alvarez-Buylla A. Chain migration of neuronal precursors. Science 1996;271:978–981. [PubMed: 8584933]

Luskin MB. Restricted proliferation and migration of postnatally generated neurons derived from the forebrain subventricular zone. Neuron 1993;11:173–189. [PubMed: 8338665]

Matsuda T, Cepko CL. Controlled expression of transgenes introduced by in vivo electroporation. Proc Natl Acad Sci USA 2007;104:1027–1032. [PubMed: 17209010]

Montana V, Ni Y, Sunjara V, Hua X, Parpura V. Vesicular glutamate transporter-dependent glutamate release from astrocytes. J Neurosci 2004;24:2633–2642. [PubMed: 15028755]

Monyer H, Burnashev N, Laurie DJ, Sakmann B, Seeburg PH. Developmental and regional expression in the rat brain and functional properties of four NMDA receptors. Neuron 1994;12:529–540. [PubMed: 7512349]

Nacher J, Varea E, Miguel Blasco-Ibanez J, Gomez-Climent MA, Castillo-Gomez E, Crespo C, Martinez-Guijarro FJ, McEwen BS. N-methyl-d-aspartate receptor expression during adult neurogenesis in the rat dentate gyrus. Neuroscience 2007;144:855–864. [PubMed: 17157994]

Nguyen L, Malgrange B, Breuskin I, Bettendorff L, Moonen G, Belachew S, Rigo JM. Autocrine/paracrine activation of the GABA(A) receptor inhibits the proliferation of neurogenic polysialylated neural cell adhesion molecule-positive (PSA-NCAM+) precursor cells from postnatal striatum. J Neurosci 2003;23:3278–3294. [PubMed: 12716935]

Peretto P, Merighi A, Fasolo A, Bonfanti L. Glial tubes in the rostral migratory stream of the adult rat. Brain Res Bull 1997;42:9–21. [PubMed: 8978930]

Petrus DS, Fabel K, Kronenberg G, Winter C, Steiner B, Kempermann G. NMDA and benzodiazepine receptors have synergistic and antagonistic effects on precursor cells in adult hippocampal neurogenesis. Eur J Neurosci 2009;29:244–252. [PubMed: 19200231]

Platel JC, Dave KA, Bordey A. Control of neuroblast production and migration by converging GABA and glutamate signals in the postnatal forebrain. J Physiol(Lond) 2008a;586:3739–3743. [PubMed: 18467361]

Platel JC, Dupuis A, Boisseau S, Villaz M, Albrieux M, Brocard J. Synchrony of spontaneous calcium activity in mouse neocortex before synaptogenesis. Eur J Neurosci 2007a;25:920–928. [PubMed: 17331190]

Platel JC, Gordon V, Heintz T, Bordey A. GFAP-GFP neural progenitors are antigenically homogeneous and anchored in their enclosed mosaic niche. Glia 2009;57:66–78. [PubMed: 18661547]

Platel JC, Lacar B, Bordey A. GABA and glutamate signaling: homeostatic control of adult forebrain neurogenesis. J Mol Histol 2007b;38:602–610. [PubMed: 18309566]

Platel J, Heintz T, Young S, Gordon V, Bordey A. Tonic activation of GLUK5 kainate receptors decreases neuroblast migration in a whole mount preparation of the subventricular zone. J Physiol(Lond) 2008b; 586:3783–3793. [PubMed: 18565997]

Rubio ME, Juiz JM. Differential distribution of synaptic endings containing glutamate, glycine, and GABA in the rat dorsal cochlear nucleus. J Comp Neurol 2004;477:253–272. [PubMed: 15305363]

Rubio ME, Wenthold RJ. Differential distribution of intracellular glutamate receptors in dendrites. J Neurosci 1999;19:5549–5562. [PubMed: 10377362]

Schiavo G, Matteoli M, Montecucco C. Neurotoxins affecting neuroexocytosis. Physiol Rev 2000;80:717–766. [PubMed: 10747206]

Snapyan M, Lemasson M, Brill MS, Blais M, Massouh M, Ninkovic J, Gravel C, Berthod F, Gotz M, Barker PA, Parent A, Saghatelyan A. Vasculature guides migrating neuronal precursors in the adult mammalian forebrain via brain-derived neurotrophic factor signaling. J Neurosci 2009;29:4172–4188. [PubMed: 19339612]

Sorensen JB. SNARE complexes prepare for membrane fusion. Trends Neurosci 2005;28:453–455. [PubMed: 15996765]

Stewart RR, Hoge GJ, Zigova T, Luskin MB. Neural progenitor cells of the neonatal rat anterior subventricular zone express functional GABA(A) receptors. J Neurobiol 2002;50:305–322. [PubMed: 11891665]

Striedinger K, Meda P, Scemes E. Exocytosis of ATP from astrocyte progenitors modulates spontaneous Ca2+ oscillations and cell migration. Glia 2007;55:652–662. [PubMed: 17309060]

Tashiro A, Sandler VM, Toni N, Zhao C, Gage FH. NMDA-receptor-mediated, cell-specific integration of new neurons in adult dentate gyrus. Nature 2006;442:929–933. [PubMed: 16906136]

Thevenaz P, Ruttimann UE, Unser M. A pyramid approach to subpixel registration based on intensity. IEEE Trans Image Process 1998;7:27–41. [PubMed: 18267377]

Wang DD, Krueger DD, Bordey A. Biophysical properties and ionic signature of neuronal progenitors of the postnatal subventricular zone *in situ*. J Neurophysiol 2003a;90:2291–2302. [PubMed: 12801891]

Wang DD, Krueger DD, Bordey A. GABA depolarizes neuronal progenitors of the postnatal subventricular zone via $GABA_A$ receptor activation. J Physiol (Lond) 2003b;550:785–800. [PubMed: 12807990]

Zhang Q, Pangrsic T, Kreft M, Krzan M, Li N, Sul JY, Halassa M, Van Bockstaele E, Zorec R, Haydon PG. Fusion-related release of glutamate from astrocytes. J Biol Chem 2004;279:12724–12733. [PubMed: 14722063]

Zhao C, Deng W, Gage FH. Mechanisms and functional implications of adult neurogenesis. Cell 2008;132:645–660. [PubMed: 18295581]

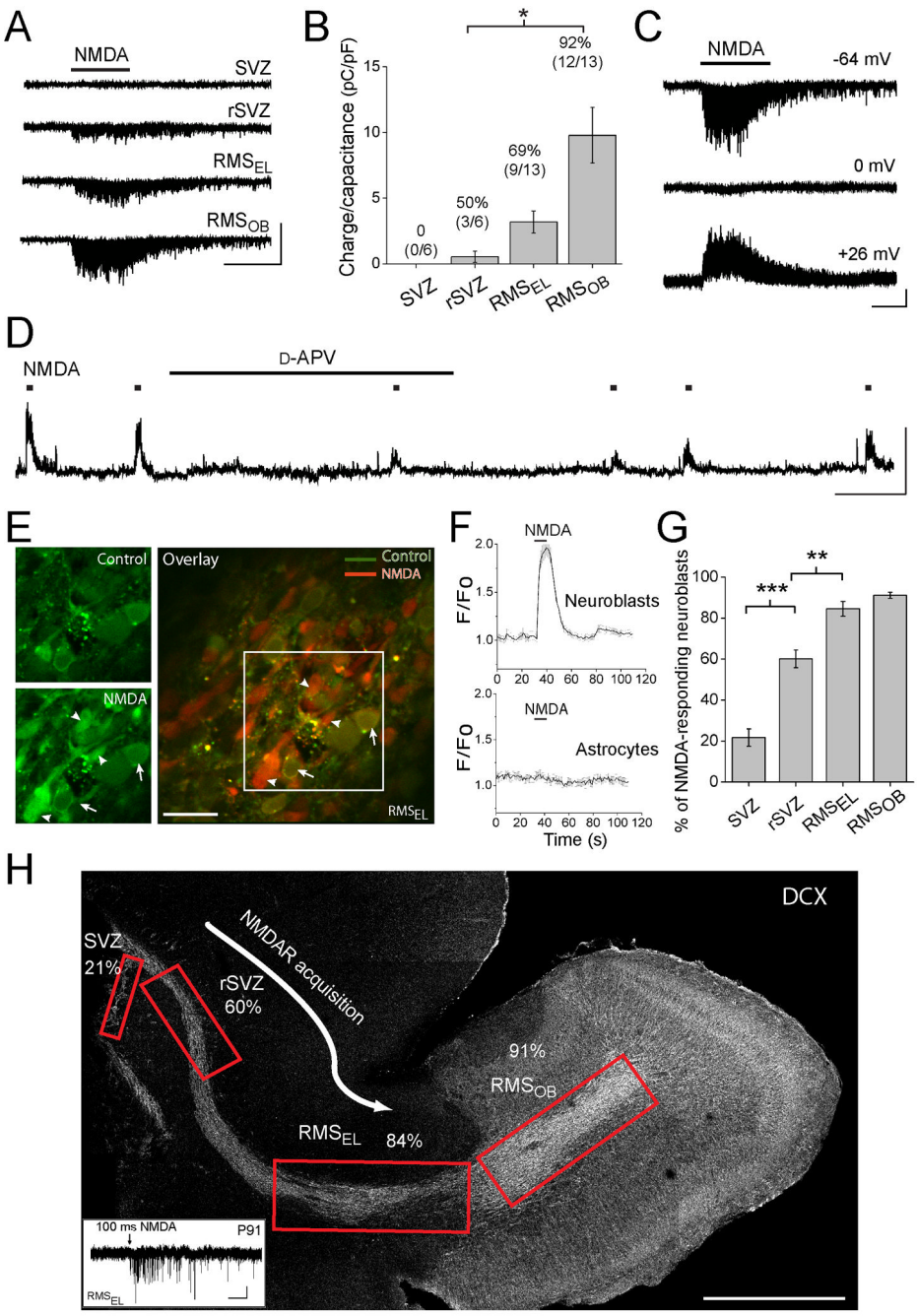

Figure 1. Neuroblasts acquire NMDARs during their migration in the rSVZ and RMS_{EL}

(A) Perforated patch clamp records of neuroblasts at different positions along the caudal-rostral axis en route to the olfactory bulb. The different locations including the SVZ along the lateral ventricle, the rostral SVZ (rSVZ), the RMS_{EL} (EL for elbow), and the RMS of the olfactory bulb (RMS_{OB}) are illustrated on a sagittal section in (H). Pressure application of 100 μM NMDA (5 s) induced inward currents in rSVZ and RMS but not SVZ neuroblasts (held at −64 mV). Scale: 10 pA/5 s. **(B)** Bar graphs illustrating NMDA-induced charge transfer divided by the cell capacitance (*, $p<0.05$). The numbers above the bars represent the percentage of neuroblast responding to NMDA at each location. **(C)** NMDA-induced currents at different holding potentials (indicated on the right). Scale: 5 pA/5 s. **(D)** NMDA-induced depolarizations

before, during, and after wash-out of 50 μM D-APV in the bath. NMDA applications are indicated by the squares over the trace. Scale: 20 mV/60 s. **(E)** Confocal images of Fluo-4 AM-loaded RMS_{EL} cells before (control) and during NMDA application (100 μM, 10 s) in an acute sagittal slice. Overlaid images (control in green and NMDA in red) is shown on the right. The arrows point to GFP-expressing cells identifying them as astrocytes. The arrowhead points to NMDA-responding neuroblasts. Scale: 20 μm. **(F)** Calcium traces from several neuroblasts and astrocytes from the slices shown in (E). NMDA (10 s) induces calcium increases in neuroblasts but not astrocytes. **(G)** Bar graphs illustrating a significant increase in the percentage of neuroblasts responding to NMDA with Ca^{2+} increases as a function of their location (**, $p<0.01$ and ***, $p<0.001$). Per location 4–11 recordings and 8–42 neuroblasts were analyzed. **(H)** Reconstructed image of a sagittal section with boxed regions showing the locations of the patch clamp and Ca^{2+} recordings. The percentage of cells that responded to NMDA with a current is indicated at each location. Scale: 500 μm. Inset: 100 μM NMDA-induced current in a RMS_{EL} neuroblast from a P91 mouse. Scale: 2 pA/1 s.

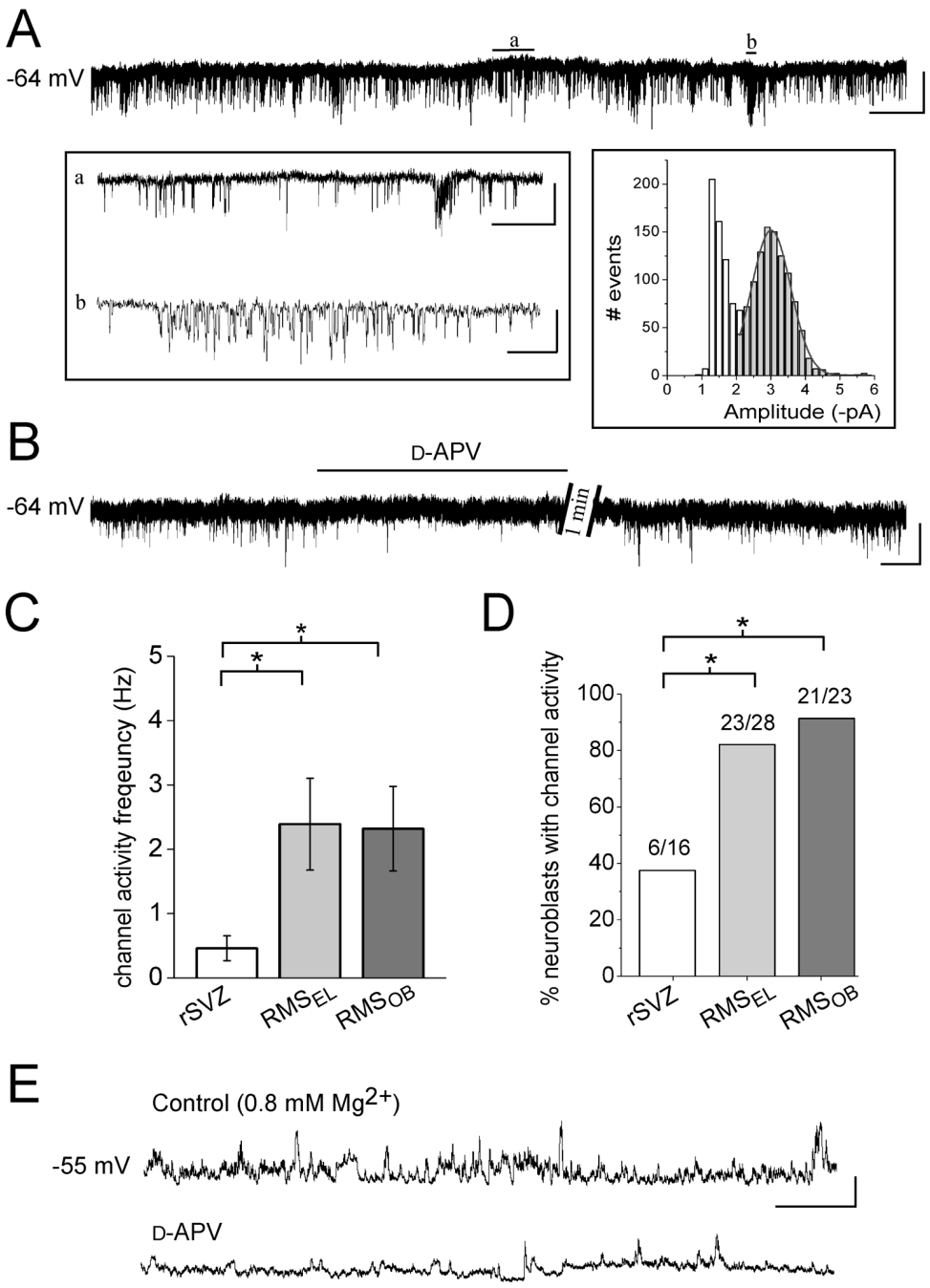

Figure 2. Most neuroblasts display phasic NMDAR activation by the time they reach the RMS_{EL}

(A) Perforated patch clamp records illustrating spontaneous single channel events (sSCEs) in a neuroblast of the RMS_{EL}. Periods (a and b) are displayed on an expanded time-scale in the left inset. The right inset represents an amplitude histogram (bin size: 0.2 pA, 1617 events) for which part of the record is shown above. A Gaussian fit yielded a mean amplitude of −3.0 pA. Scale bars: 5 pA/4 s, 400 ms (a), 50 ms (b). **(B)** Perforated patch clamp records illustrating that sSCEs are sensitive to D-APV. Scale: 5 pA/30 s. **(C)** Bar graphs representing the frequency of single channels in rSVZ, RMS_{EL}, and RMS_{OB} neuroblasts (n=6, 17, and 20, respectively). The frequency significantly increased from the rSVZ to the RMS_{EL} and to the RMS_{OB} ($p<0.05$). **(D)** Bar graphs illustrating a significant increase in the percentage of neuroblasts displaying

sSCEs from the rSVZ to the RMS_{EL} ($p<0.05$). **(E)** Perforated patch clamp recordings in current clamp illustrating spontaneous depolarizations sensitive to D-APV in aCSF with near-physiological Mg^{2+} concentration (0.8 mM). Scale: 10 mV/3 s.

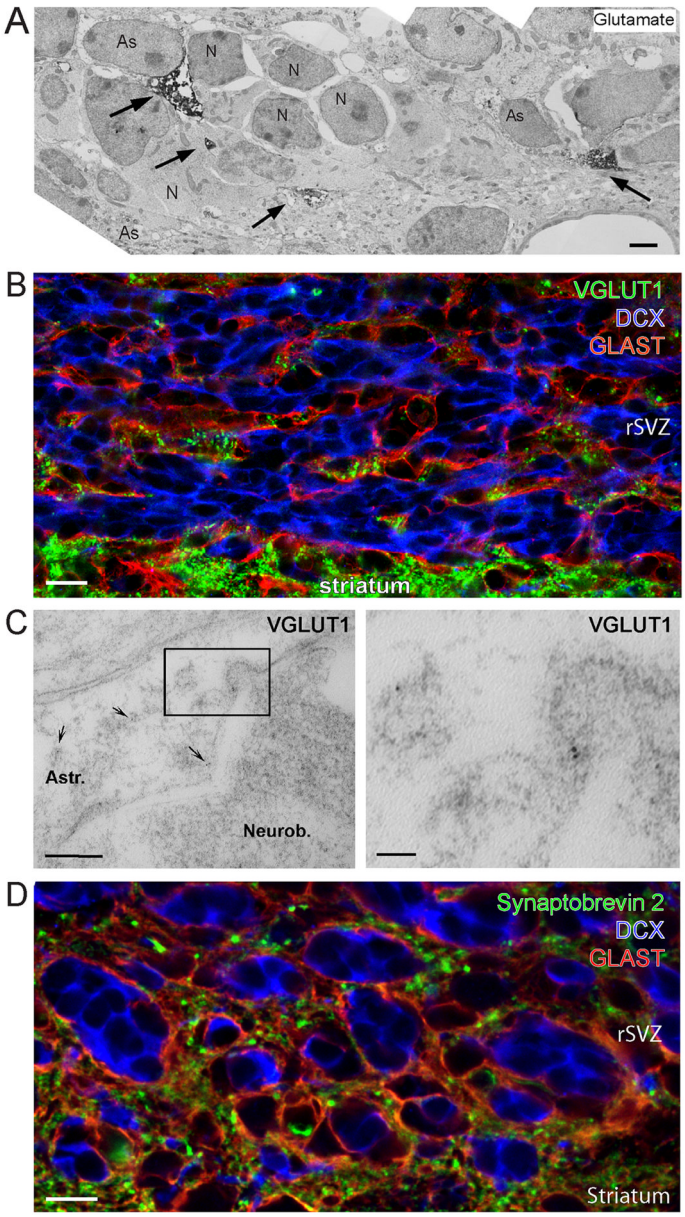

Figure 3. VGLUT1 and Synaptobrevin 2 are only expressed in astrocytes in the SVZ/RMS

(A) Electron micrograph of pre-embedding immunocytochemistry for L-glutamate in the rSVZ. The electron dense material for glutamate (as indicated by the arrows) is observed exclusively in astrocytes (As) surrounding neuroblasts (N). Scale: 1 μm. **(B)** Confocal image displaying co-immunostaining for VGLUT1 (green), doublecortin (DCX, blue), and GLAST (red) in the RMS. Scale: 10 μm. **(C)** Electron micrographs showing post-embedding immunocytochemistry for VGLUT1 expression in the rSVZ. The right panel represents a higher magnification image of the boxed region shown in the left panel. The secondary antibody was conjugated to 5 nm-gold particles (arrows). Scale bars: 200 nm (left)/50 nm (right). **(D)** Confocal image of synaptobrevin 2 (green), DCX (blue), and GLAST (red). Scale: 10 μm.

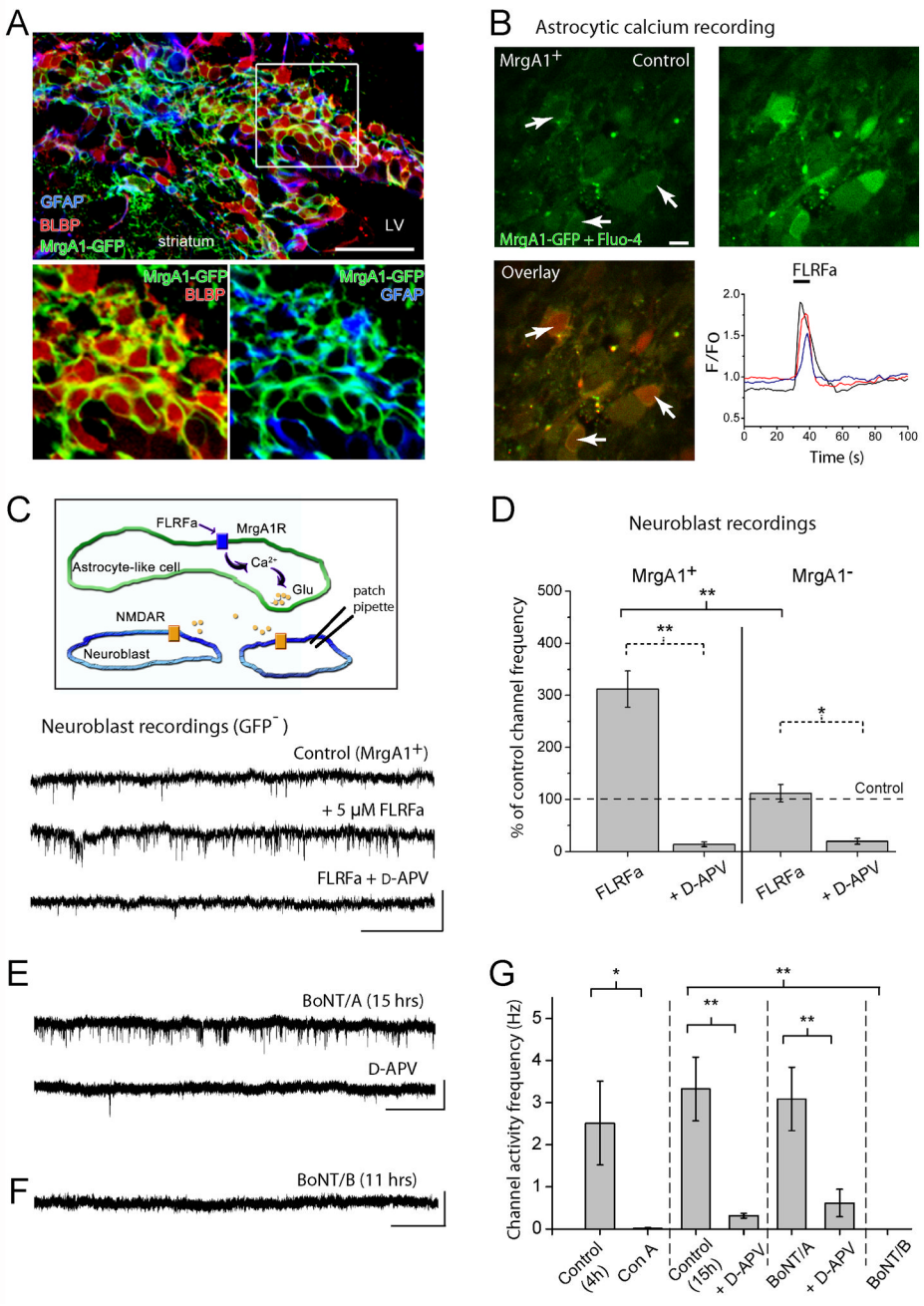

Figure 4. Ca^{2+}-dependent vesicular glutamate release from RMS astrocytes contributes to NMDAR activation in neuroblasts

(A) Confocal image displaying co-immunostaining for GFP in $MrgA1^+$ mice (green), GFAP (blue), and BLBP (red) in the SVZ. The inset illustrates GFP/BLBP and GFP/GFAP staining from the image in the boxed region. Scale bars: 70 µm (top image)/40 µm. **(B)** Top: Confocal images of GFP- and Fluo-4-fluorescent cells in the RMS before (control) and during FLRFa pressure application (5 µM, 10 s). Recordings were performed in the RMS in acute sagittal slices from a $MrgA1^+$ mouse. The arrow indicates astrocytes that are outlined by GFP fluorescence. Scale: 10 µm. Bottom: Overlay of the images under control (green) and during FLRFa application (red). On the right, activity graph illustrating Ca^{2+} increases in GFP^+ cells, *i.e.* astrocytes. **(C)** Top: Model illustrating that FLRFa is applied to induce Ca^{2+} increases in

astrocytes and examine whether NMDARs are activated in adjacent neuroblasts. Bottom: Perforated patch clamp records displaying sSCEs in neuroblasts under control and in the presence of FLRFa (5 μM, bath) followed by D-APV addition in slices from $MrgA1^{+}$ mice. Scale bars: 5 pA/1 s. **(D)** Bar graphs illustrating the % increase of sSCE frequency in the presence of FLRFa without and with D-APV in $MrgA1^{+}$ mice and control single transgenic mice (tetO-MrgA1, $MrgA1^{-}$). The asterisks indicate significant enhancement above control levels of 100% (*, $p<0.05$; **, $p<0.01$). **(E)** Perforated patch clamp records displaying spontaneous SCEs in neuroblasts after 15 hrs pre-incubation in BoNT/A and after addition of D-APV. Scale: 5 pA/3 s. **(F)** Perforated patch clamp records displaying the lack of spontaneous SCEs in neuroblasts after 11 hrs pre-incubation in BoNT/B. Application of NMDA still induced inward currents. Scale: 5 pA/4 s. **(G)** Bar graphs illustrating the frequency of spontaneous SCEs following pre-incubation in control aCSF (for 4 hrs or 11–15 hrs) or BoNT/A, and the absence of SCEs following pre-incubation in Con A or BoNT/B. (** $p<0.01$, * $p<0.05$).

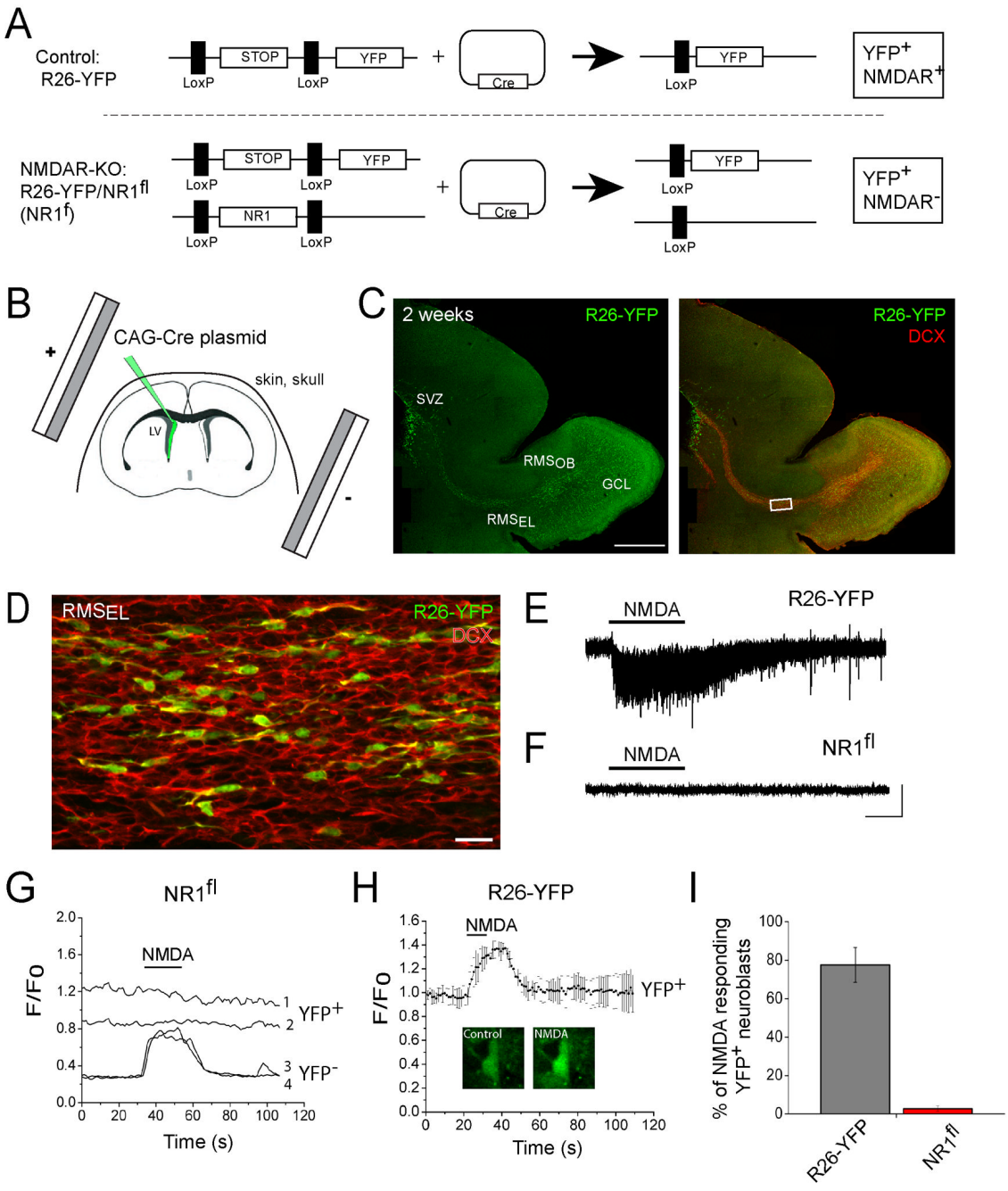

Figure 5. Single-cell knockout of functional NMDARs in neuroblasts using *in vivo* postnatal electroporation

(A) Diagram illustrating the effect of Cre expression in cells from R26R-YFP (control) and R26R-YFP/NR1^{fl} mice (NR1^{fl}) resulting in YFP$^+$ cells expressing NMDARs and in YFP$^+$ NMDAR-deficient cells, respectively. **(B)** Diagram illustrating the *in vivo* electroporation procedure in neonatal R26R-YFP mice. **(C)** Reconstructed confocal image of a sagittal section that contained DCX-immunopositive (red) YFP-expressing cells (green). Scale: 500 μm. **(D)** Confocal image of YFP (green) and DCX (red) staining from the boxed image in (C). Scale: 30 μm. **(E and F)** Whole cell patch clamp records of YFP$^+$ neuroblasts in R26-YFP (E) and R26-YFP/NR1^{fl} mice. Application of 100 μM NMDA (10 s) induced inward currents in

neuroblasts of control R26-YFP mice, but not in neuroblasts of R26-YFP/NR1^{fl} mice. Scale: 25 pA/5 s. **(G)** Ca^{2+} activity graph from YFP^{+} and YFP^{-} neuroblasts in the RMS from a R26R-YFP/NR1^{fl} mouse. **(H)** Mean NMDA-induced Ca^{2+} responses in YFP^{+} neuroblasts from control R26R-YFP mice. A YFP^{+}/Fluo-4 AM^{+} cell before and during NMDA application is shown under the Ca^{2+} trace. **(I)** Bar graphs illustrating the % of YFP^{+} neuroblasts responding to NMDA in the RMS in acute sagittal slices from R26R-YFP and NR1^{fl} mice.

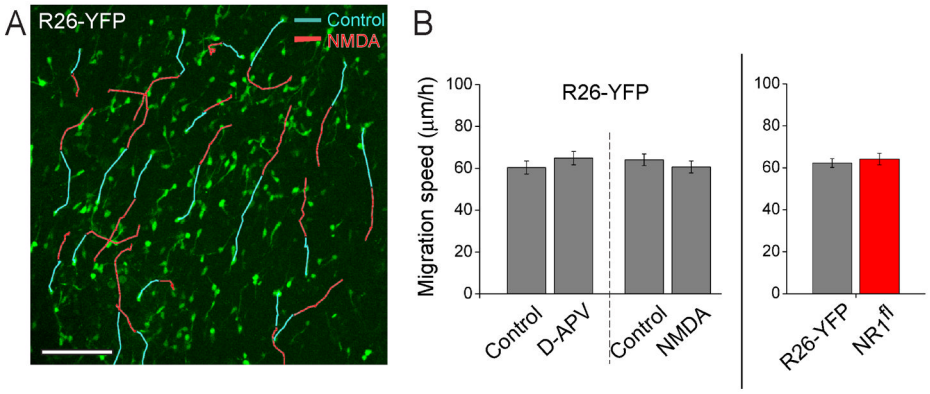

Figure 6. NMDAR does not regulate neuroblast migration

(A) Examples of migratory routes of individual neuroblasts in the RMS_{EL} of a R26-YFP mouse before (blue lines) and during NMDA application (10 μM, red lines). The underlaid image is the first time point of acquisition. Scale: 100 μm. **(B)** Bar graphs illustrating the average speed of neuroblast migration under control conditions and in the presence of D-APV (50 μM) or NMDA (10 μM) in R26-YFP mice, and under control conditions in slices from R26-YFP versus $NR1^{fl}$ mice.

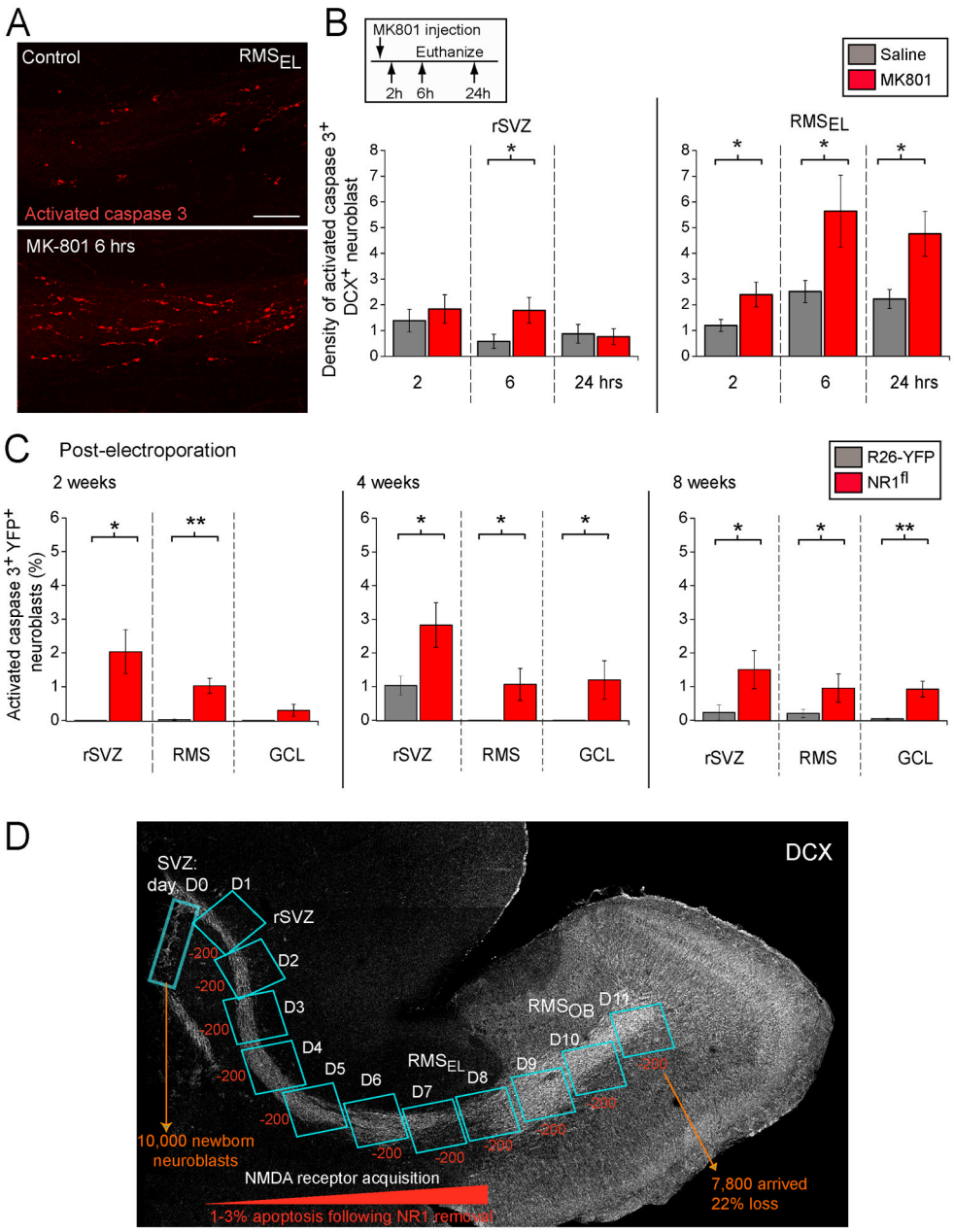

Figure 7. *In vivo* blockade and genetic removal of NMDARs decrease neuroblast survival

(A) Confocal images displaying immunostaining for activated caspase 3 (red) in the RMS from control or MK-801-treated *DCX*-GFP mice. Scale: 100 μm. **(B)** Bar graphs of the density of activated caspase 3-immunopositive DCX^+ cells in sagittal slices containing the rSVZ and RMS_{EL} following *in vivo* injections of saline solution (Ctl) or MK-801. Mice received a single dose of MK-801 and were sacrificed at different time-points following injection (2, 6, and 24 hrs). The density was obtained by dividing the cell number by the volume of the region analyzed. The inset illustrates the experimental paradigm. **(C)** Bar graphs of the percentage of activated caspase 3^+ YFP^+/DCX^+ neuroblasts in the rSVZ, RMS and granule cell layer (GCL) of the OB quantified at 2, 4, and 8 weeks post-electroporation. The % was calculated from the total number of YFP^+ neuroblasts. **(D)** Model illustrating the predicted effect of increased apoptosis on accumulated cell loss along the migratory route. Considering that ~10,000

neuroblasts are born per day, ~200 NR1-KO neuroblasts (1–3%) will be apoptotic and cleared in ~1 day. Since its takes ~11 days for newly born neuroblasts to migrate from the SVZ to the RMS_{OB}, apoptosis would lead to a total loss of ~2,200 neuroblasts in the RMS_{OB}, corresponding to 22% of the original neuroblast population.

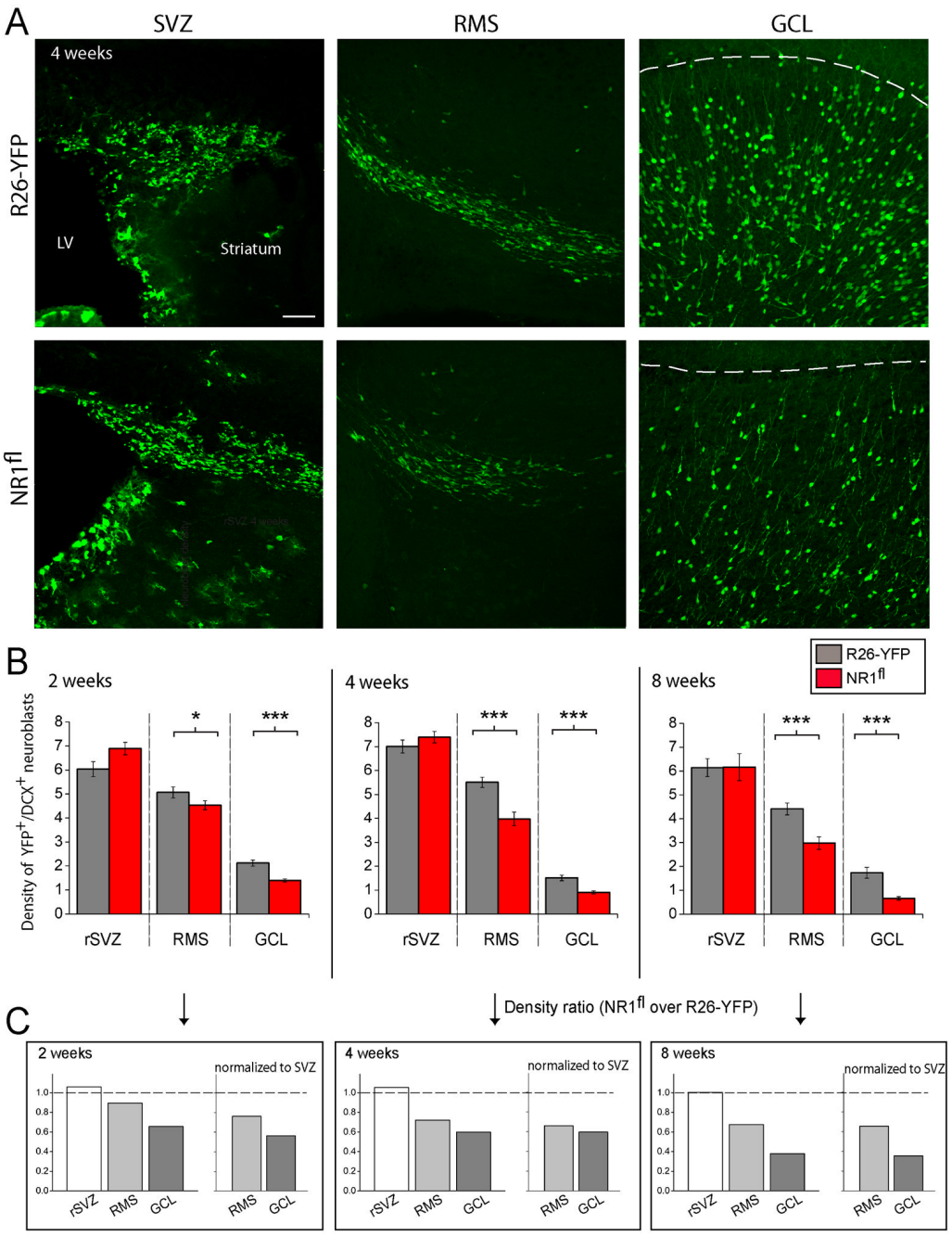

Figure 8. Single neuroblast knockout of NR1 results in neurogenesis deficit

(A) Confocal images of YFP^+ cells in the SVZ, RMS and GCL in sections from R26R-YFP and R26R-YFP/$NR1^{fl}$ mice. Scale: 70 μm. The dashed line indicates the location of the mitral cell layer. **(B)** Bar graphs of the density of YFP^+/DCX^+ cells (*i.e.* YFP^+ neuroblasts) in the rSVZ, RMS and granule cell layer of the OB (GCL) quantified at 2, 4, and 8 weeks post-electroporation. Experiments were performed in R26R-YFP (i.e. control) and R26R-YFP/$NR1^{fl}$ mice ($NR1^{fl}$, 4–5 mice for each data point) at 2, 4 and 8 weeks. (* $p<0.05$, ** $p<0.01$, *** $p<0.001$). **(C)** Bar graphs of density ratios obtained by dividing the density in $NR1^{fl}$ by that in R26-YFP mice before and following normalization by the density of YFP-expressing cells in the SVZ/rSVZ of the same animal.